# Manipulating regioregular poly(3-hexylthiophene) : [6,6]-phenyl-$C_{61}$-butyric acid methyl ester blends—route towards high efficiency polymer solar cells†

**Gang Li,[a] Vishal Shrotriya,[b] Yan Yao,[a] Jinsong Huang[a] and Yang Yang*[a]**

***Received 28th February 2007, Accepted 25th May 2007***
***First published as an Advance Article on the web 11th June 2007***
**DOI: 10.1039/b703075b**

Polymer or "plastics" solar cells have been an intensively studied area since the discovery of efficient electron transfer between polymers and fullerenes and the introduction of the bulk-heterojunction concept. The last few years have seen significant improvement in plastic solar cell performance through aggressive research on the regioregular poly(3-hexylthiophene) (RR-P3HT) : [6,6]-phenyl-$C_{61}$-butyric acid methyl ester (PCBM) system. The morphology of the system is controlled through two major strategies which have proven effective in improving the device efficiency—thermal annealing and solvent annealing (slow growth). In this Feature Article, we review the recent progress on this material system. A detailed discussion on thermal annealing and solvent annealing approaches to improve device performance is presented, including a comparison between the two strategies. The effects of these two approaches on improving polymer crystallinity, light absorption in the polymer, carrier transport, blend film nano-morphology, *etc.* are summarized. We also include a brief discussion on accurate measurement and characterization techniques for polymer solar cells to correctly determine the efficiency by applying spectral mismatch factors. Future directions and challenges on polymer solar cell development are also discussed.

## 1. Introduction

Since the beginning of the industrial revolution in the 18th century, our ability to generate, store, and utilize energy from various sources has played a major role in our progress. Electricity is one of the most versatile and ubiquitous forms of energy available to humans. However, our ever growing population and rapidly developing economies are creating an ever increasing gap in supply and demand of electricity. Fossil

[a]*Department of Materials Science and Engineering, University of California Los Angeles, Los Angeles, California 90095, USA. E-mail: yangy@ucla.edu*
[b]*Solarmer Energy, Inc., El Monte, California 91731, USA*
† This paper is part of a *Journal of Materials Chemistry* theme issue on New Energy Materials. Guest editor: M. Saiful Islam.

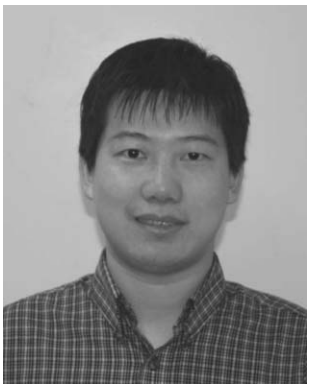

**Yan Yao**

*Yan Yao has been a Ph.D. candidate in the Department of Materials Science and Engineering at University of California, Los Angeles, under the supervision of Professor Yang Yang since 2003. He obtained a B.S. and a M.S. at Fudan University (China) in 2000 and 2003, respectively. His main research activities are in the field of organic optoelectronics with a focus on polymer solar cells.*

**Gang Li**

*Gang Li has been a postdoctoral researcher in Prof. Yang Yang's group in the Department of Materials Science and Engineering at UCLA since 2004. He obtained a B.S. at Wuhan University (China) in 1994, and a Ph.D. in Condensed Matter Physics at Iowa State University in 2003 focusing on organic light-emitting devices (OLEDs). His current research focus is on polymer solar cells.*

**Vishal Shrotriya**

*Vishal Shrotriya is a Technology Researcher at Solarmer Energy, Inc., based in El Monte, CA. He obtained his B.S. degree in Metalurgical Engineering and Materials Science from Indian Institute of Technology, Bombay in 2002, and M.S. and Ph.D. in Materials Science and Engineering from UCLA in 2004 and 2007, respectively. In his doctoral research he focussed on high efficiency polymer photovoltaic cells based on polymers.*



 

fuels provide most of the energy consumed by human beings. Burning of fossil fuels brings environmental problems, and the availability of fossil fuels is becoming less by the day. To meet the energy demands of the world in the 21st century, it is necessary to develop affordable renewable energy sources.[1] The sun deposits 120 000 TW of power onto the Earth's surface, which is far more than enough to provide the 13 TW of total power that is currently used by the planet's population, or the 30 TW that will probably be needed by 2050.[2] Photovoltaics—the technology to generate electrical power from semiconductors when they are illuminated by sunlight—is one of the most promising of such sources. Although the first functional photovoltaic (PV) devices was made in 1883,[3] it was in 1954 that the first efficient solar cell was reported at Bell Labs,[4] and heralded the arrival of the modern photovoltaics era. From the mid-1960s to mid-1980s, the focus of research on PV was on improving the efficiency to produce more power. During the 1990s, the average growth rate of PV production was over 33% per annum.[5] Crystalline silicon (Si) is used as the semiconductor component in over 90% of the PV applications today. Other materials and technologies such as amorphous silicon (a-Si), copper indium gallium arsenide (CIGS), cadmium telluride (CdTe), *etc.* have also been explored.[5]

However, after all the research and development and the promise of PV technology, only about 0.1% of total electricity generated in the world is supplied from PV installations.[6] The primary reasons for this are the high cost of raw materials and processing, and difficulty in fabrication and installation of PV systems. Serious rethinking on the research direction of PV technology is required to overcome these barriers and make PV an economically viable alternative for wider acceptance. As a result, the primary goal of PV research today is to produce economically efficient PV system, through low cost materials that give high efficiency. Some of the technological goals of current solar cell research and manufacturing are to use less semiconductor materials by adopting thin film structures, or use less expensive semiconductor materials, improve solar cell performance for less expensive semiconductor materials, increase solar radiation utilization by increasing absorption of the solar spectrum, and simplifying processing, reducing fabrication costs and increasing the yield.

The discovery of organic electronic materials[7] opened a new direction of research in several electronic devices, such as light emitting diodes,[8,9] thin-film transistors,[10–12] memory devices,[13,14] and solar cells.[15,16] Today, solar cells based on organic materials and polymers are considered promising alternatives to their inorganic counterparts.[11,12] Some of the advantages of organic solar cells are low-cost fabrication of large-area devices, low specific weight, mechanical flexibility, and easy tunability of chemical properties of the organic materials.[15,16] Polymeric solar cells, due to easy solution processing, are especially attractive to harness solar energy in a cost effective way. Significant efforts are under way to improve their efficiency to the level of practical applications. However, for all these advantages associated with this novel technology, the efficiency of polymer solar cells is still relatively low compared to inorganic solar cells. Device efficiencies of 4–5% have been reported to date.[17] This implies that a significant amount of research is required to bring this technology out from the research labs to the market. It is widely believed that the efficiency barrier of 10% has to be crossed before polymer solar cells are commercialized.[18]

## 2. Energy conversion in polymer solar cells—scope for improvement

Before discussing the methods to improve the performance or energy conversion efficiency of polymer solar cells, it is important to understand the physics that is involved in the conversion of light to electricity in a typical polymer solar cell. The energy conversion, or photovoltaic, process in a polymer solar cell is a multiple step process,[19] as follows. *Step 1—Incoupling of the photon*: The incoming photons encounter the first interface—glass or plastics—when they hit the device. The reflection losses at the air/substrate interface as well as at each subsequent interface, which depend on the difference between optical refractive indices of the two materials, have to be minimized. *Step 2—Photon absorption*: The incoming photons are then absorbed in the active layer. The absorption spectrum of the active material should match the solar irradiation for maximum absorption. As a result, low band-gap polymers are highly desired. *Step 3—Exciton formation and migration*: After a photon has been absorbed in the polymer, an exciton is formed. The excitons then diffuse in the material with a characteristic exciton diffusion length ($L_D$) typically of the order of 5–10 nm.[20,21] $L_D$ depends on the structure of the

**Jinsong Huang**

*Jinsong Huang has been a Ph.D. student in Prof. Yang Yang's group in the Department of Materials Science and Engineering at UCLA since 2003. His research at UCLA focuses on high performance polymer based solar cells and light emitting diodes.*

*Yang Yang received a B.S. at National Cheng Kung University, Taiwan in 1982, and a Ph.D. at University of Massachusetts-Lowell (Physics and Applied Physics) in 1991.*

**Yang Yang**

*After one year postdoctoral experience at University of California-Riverside in the field of Physical Chemistry, he worked on organic semiconductor devices in UNIAX Corporation from 1992 to 1996. He became a member of the UCLA faculty in the Department of Materials Science and Engineering in 1997 and has been a full professor since 2002. He has published more than 150 articles in peer-reviewed journals.*

material and the dielectric properties. The excitons have a finite lifetime and during the diffusion they decay or dissociate through several mechanism. In order to achieve efficient photovoltaic conversion, the excitons have to be dissociated into free electrons and holes, before they decay radiatively, thermally or vibronically. *Step 4—Exciton dissociation or charge separation*: The most common way to achieve exciton dissociation into free electrons and holes is through photo-induced charge transfer process. The processes that act as counterforces to exciton dissociation are geminate recombination, where separated electrons and holes recombine back to form an exciton, and non-geminate bimolecular recombination, where an electron and a hole from different excitons recombine. *Step 5—Charge transport*: The free charges must then travel through the active layer to reach the electrodes where they can be collected to produce photocurrent. The charge carrier mobilities for both electron and hole therefore play an important role in determining device efficiency. The charge carrier mobility in conjugated polymers is usually very low,[10,22,23] which makes it necessary to have a thin active layer, which on the other hand reduces the optical absorption. *Step 6—Charge collection*: Finally, the free electrons that reach the electrodes are collected and passed into the outer circuit to generate device photocurrent. The charge collection efficiency depends on the energy level matching at the metal/polymer interface, interfacial defects, *etc.*

In this Feature Article, we will focus on the internal properties of the active polymer blend layer in a typical planar polymer solar cell structure. In other words we neglect the roles of steps 1 and 6 for efficiency enhancement and focus on the other steps. The existence of ultra-fast charge transfer ($\sim$40 fs) has been demonstrated in conjugated polymer and fullerene derivative systems (bilayer or blend) by using pump–probe techniques,[24,25] which gives a photo-induced charge transfer (*Step 4*) efficiency close to 100% in an appropriately selected polymer–fullerene system. Furthermore, introduction of the bulk-heterojunction (BHJ)[26,27] concept represented a milestone in the development of polymer based solar cells. With distributed donor/acceptor interfaces within the entire volume of the composite layer in BHJ the limitations of exciton migration (*Step 3*) and charge separation (*Step 4*) are overcome. As a result, the two most important areas of improvement in polymer solar cells are light absorption in the polymer (*Step 2*) and charge carrier transport in the active layer (*Step 5*). In this Feature Article, we will review the recent results and developments from various research groups on these two promising fronts. The role of two approaches mentioned earlier, thermal annealing and solvent annealing, is investigated in detail to provide the readers with an overall understanding of how these approaches result in a significant improvement in polymer solar cell efficiency.

## 3. Accurate measurement of efficiency—spectral mismatch factor

As in the case of any new technology which is undergoing rapid progress, standardization is a crucial step for its further development. For healthy development of polymer solar cell technology, it is critical to accurately determine the efficiency values for a fair comparison with results among various research groups. Significant efforts have been made in the past to accurately determine the efficiency of solar cells, and a standard test method has been established.[28] For calibration and measurement purpose, two types of P3HT : PCBM blend solutions were prepared—1 : 1 wt. ratio (20 mg ml$^{-1}$ P3HT) in dichlorobenzene (DCB)[17a] and 1 : 0.8 wt. ratio (10 mg ml$^{-1}$ P3HT) in chlorobenzene (CB)[17b,c]—to fabricate two types of devices named P3HT : PCBM(DCB) and P3HT : PCBM(CB), respectively. Solar cells using poly[2-methoxy-5-(2′-ethyl-hexyloxy)-1,4-phenylene vinylene] (MEH-PPV) were also fabricated with a MEH-PPV : PCBM weight ratio of 1 : 4 and DCB as solvent.[29]

The current reference spectrum adopted by the international terrestrial PV community is given in Standard IEC 60904-3 (*Measurement principles for terrestrial PV solar devices with reference spectral irradiance data*, International Electrotechnical Commission, Geneva) and ASTM Standard G159 (*Standard tables for reference solar spectral irradiances: direct normal and hemispherical on 37° tilted surface*, American Society for Testing and Materials, West Conshacken, PA). The irradiance incident on the PV cell is typically measured with a reference cell. For *I–V* measurements with respect to a reference spectrum, there is a spectral error in the measured $I_{SC}$ of the PV cell because of the following two reasons: (i) the spectral irradiance of the light source does not match the reference spectrum, which is computer generated, and (ii) the spectral responses of reference detector and test cell are different. This error can be derived based upon the assumption that the photocurrent is the integral of the product of cell responsivity and incident spectral irradiance. This error can be expressed as spectral mismatch correction factor ($M$):[30]

$$M = \frac{\int_{\lambda_1}^{\lambda_2} E_{\mathrm{Ref}}(\lambda) S_{\mathrm{R}}(\lambda)\mathrm{d}\lambda \int_{\lambda_1}^{\lambda_2} E_{\mathrm{S}}(\lambda) S_{\mathrm{T}}(\lambda)\mathrm{d}\lambda}{\int_{\lambda_1}^{\lambda_2} E_{\mathrm{Ref}}(\lambda) S_{\mathrm{T}}(\lambda)\mathrm{d}\lambda \int_{\lambda_1}^{\lambda_2} E_{\mathrm{S}}(\lambda) S_{\mathrm{R}}(\lambda)\mathrm{d}\lambda} \quad (1)$$

where $E_{\mathrm{Ref}}(\lambda)$ is the reference spectral irradiance, $E_{\mathrm{S}}(\lambda)$ is the source spectral irradiance, $S_{\mathrm{R}}(\lambda)$ is the spectral responsivity of the reference cell, and $S_{\mathrm{T}}(\lambda)$ is the spectral responsivity of the test cell, each as a function of wavelength ($\lambda$). A matched photovoltaic reference cell is typically used as the reference detector and a solar simulator is used as the light source to minimize the deviation of $M$ from unity. Once $M$ is known, the measured photocurrent needs to be scaled by dividing $M$ to obtain the photocurrent under AM1.5G standard testing conditions. For the purpose of light-source calibration for organic solar cell testing, a reference cell with a spectral response matching that of the actual test cells is preferred to minimize the spectral error which is not being numerically corrected for. The spectral responsivities of three reference cells are shown in Fig. 1a: the unfiltered Si diode shows significant response in the wavelength range of 400–1100 nm; and the response for a Si diode with KG5 color filter is exhibited in the wavelength range of 350–700 nm, making it more suitable for use in calibrating the light intensity of the solar simulator. The reference spectrum used is the AM1.5G standard spectrum and the source irradiance spectrum is the

 

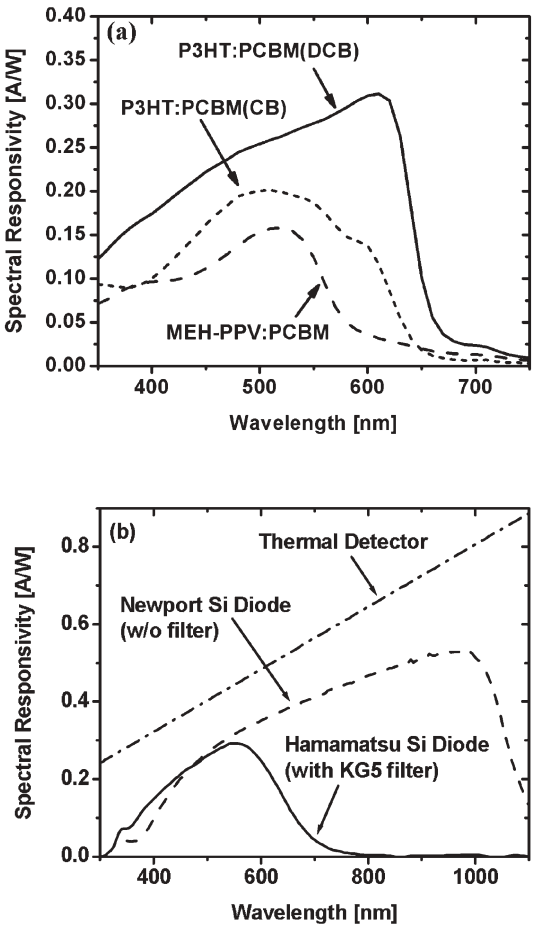


**Fig. 1** (a) The spectral responsivities [$S_T(\lambda)$] for three types of test cells: MEH-PPV : PCBM, P3HT : PCBM(CB), and P3HT : PCBM(DCB). (b) Spectral responsivities of three types of reference cells: unfiltered monocrystalline Si diode, Si diode with KG5 color filter, and thermal detector. (Reprinted with permission from reference 29, copyright 2006, Wiley VCH.)

typical irradiance spectrum for Oriel 150 W solar simulator with AM1.5G filter (Newport Corporation). The reference and the source spectra used for calculating $M$ are shown in Fig. 1b. The $M$ values calculated for different test cell/reference cell combinations are summarized in Table 1. Using a Si diode with KG5 color filter as a reference cell for light-source calibration has a clear advantage over an unfiltered Si diode and a thermal detector. The mismatch-factor values are very close to unity when a KG5 filtered Si diode is used as the reference cell, whereas the mismatch is 31–35% for an unfiltered Si diode and 33–37% for a thermal detector. It is therefore very important to consider the spectral mismatch and include it in efficiency calculations when reported by the organic solar cell research community.

**Table 1** Spectral mismatch factors calculated with respect to the AM1.5G reference spectrum (IEC 60904) for various test cell/reference cell combinations

| | Mismatch factors for different reference cells | | |
|---|---|---|---|
| Test cell type | KG5 color filtered | Unfiltered | Thermal detector |
| MEH-PPV : PCBM | 0.99 | 1.32 | 1.35 |
| P3HT : PCBM(CB) | 1.01 | 1.35 | 1.37 |
| P3HT : PCBM(DCB) | 1.01 | 1.35 | 1.37 |

## 4. RR-P3HT : PCBM bulk-heterojunction system

Two of the most widely studied polymer : fullerene BHJ systems for application as active layer in polymer solar cells are poly[2-methoxy-5-(3,7-dimethyloctyloxy)-1,4-phenylene vinylene] (MDMO-PPV) : PCBM[31,32] and RR-P3HT : PCBM, which represent the state-of-art polymer solar cell technology. A significant amount of research has been dedicated to these two material systems and some of the highest efficiency values have been reported for them. There are excellent review papers on the MDMO-PPV : PCBM system in the literature.[33] In this Feature Article we will focus on the recent improvements in the RR-P3HT : PCBM system, especially the approaches to optimize the active blend layer for enhancing device efficiency.

The solar irradiation spectrum extends well beyond 1 μm wavelength. One of the major problems in polymer solar cells is the insufficient absorption of the polymer in the solar irradiance spectrum. For example, the well studied polymers MDMO-PPV and MEH-PPV both exhibit absorption edges at ~550 nm, corresponding to an energy band gap of about 2.2 eV. More recently, the focus has shifted towards highly regioregular poly(3-alkylthiophenes) (P3ATs), especially RR-P3HT,[34] as the active polymer which has improved solar light harvesting, with the RR-P3HT absorption edge at ~650 nm matching well with the strongest solar spectrum. In addition, RR-P3HT has the best charge transport properties among the conjugated polymers. It is a promising candidate for polymer field effect transistors (FETs) demonstrating hole mobilities up to 0.1 $cm^2\ V^{-1}\ s^{-1}$.[11,12,35] Pure films of RR-P3HT are shown to be composed of microcrystalline domains embedded in an amorphous matrix by X-ray diffraction analysis. Inside the microcrystalline regions, P3HT chains π-stack and form lamellae of interlocking side chains. The inter-chain interactions not only facilitates the enhancement in charge carrier mobility, it is also the source of the lowest energy (longest wavelength) feature in the polymer absorption spectrum.[36]

The application of RR-P3HT to improve polymer solar cell performance, however, is not straightforward. Fig. 2 shows the ultraviolet-visible (UV-Vis) absorption spectra for pure RR-P3HT and RR-P3HT : PCBM blend films with different concentrations of PCBM.[37] The films are spin-cast at 3000 rpm for 1 minute in a nitrogen filled glove box. The solvent is removed very fast during spin-coating and polymer blend films with very smooth surfaces are produced. For the pure P3HT film the solid-state absorption spectrum shows three features—two peaks and one shoulder at the longest wavelength. The first two bands can be attributed to the π–π* transition, whereas the shoulder is due to the inter-chain interactions. The absorption of the films with increasing amount of PCBM reduces significantly in the visible range, specifically between 450–600 nm which is the peak absorption range for RR-P3HT. The modification of the absorption spectra in the films with PCBM can be attributed to the interaction between the polymer chains and PCBM molecules where the presence of

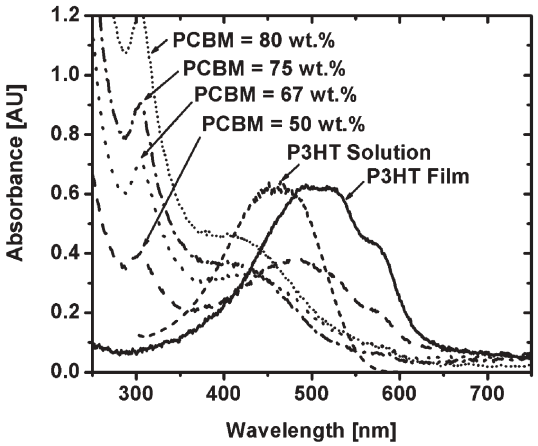


**Fig. 2** Absorption of RR-P3HT solution and RR-P3HT : PCBM blend films with different weight ratios of PCBM. (Reprinted with permission from reference 37, copyright 2005, Elsevier.)

PCBM molecules lowers the interaction among the P3HT chains upon increased disordering in the blend films.[38]

Since the donor/acceptor (D/A) blend is critical, strategies must be developed to improve light harvesting and improve charge carrier transport in the RR-P3HT : PCBM system for enhanced polymer solar cell performance. Over the last few years, research efforts have led to two highly effective approaches towards this end. One approach is thermal annealing of the polymer : fullerene films or completed devices, and the second, and more recently proposed, approach is solvent annealing (or slow growth). In this Feature Article, we will focus on the recent progress in these two approaches, and shed some light on the whole picture of the P3HT : PCBM system.

### 4.1. Thermal annealing

In their study of electroluminescence in polythiophene derivatives, Berggren *et al.* showed that thermal annealing can enhance the polymer crystallinity.[39] A DSC study on RR-P3HT conducted by Zhao *et al.* indicates that the crystalline states start to appear at annealing temperature as low as 40 °C.[40] Mild thermal treatment at 55 °C was shown to improve the efficiency of P3HT : fulleropyrrolidine solar cells from 0.1% to 0.6% by Camaioni *et al.*[41] Dittmer *et al.* studied photovoltaic cells with P3HT and a small molecule dye *N*,*N*′-bis(1-ethypropyl)-3,4:9,10-perylylene bis(tetracarboxyl diimide) (EP-PTC) as electron donor and acceptor, respectively.[42] It was observed that thermal annealing at 80 °C for 1 hour led to the highest external quantum efficiency (EQE) of 11%, an improvement by a factor of 1.6 compared to an untreated device. In 2003, Padinger *et al.*[43] reported 3.5% power conversion efficiency (PCE) polymer solar cells by annealing a RR-P3HT : PCBM blend. The demonstration of this high efficiency stimulated extensive studies on the thermal annealing approach and PCE values up to 5% were reported.[17*b*–*d*,38,44–46] While direct comparison of efficiency among different groups is difficult due to the lack of common measurement standards and missing spectral mismatch correction in most cases, significant improvement in device performance upon thermal annealing in the P3HT : PCBM system is clearly the central theme in all these studies. In the following sections we discuss some of the important mechanisms through which the improvement in device performance is achieved in this system by the thermal annealing approach. We will discuss the effect of thermal annealing on absorption, polymer crystallinity, morphology, and D/A phase separation, and the effect of film composition and active layer thickness on device performance.

**4.1a. The improvement of absorption.** As a result of enhanced P3HT crystallization upon thermal annealing, the P3HT absorption shows significant improvement. The effect of thermal annealing on polymer crystallization is discussed in the following section. Fig. 3 shows the UV-Vis absorption spectra obtained for P3HT : PCBM thin films (thickness ~ 80 nm; PCBM conc. = 50 wt%) before and after annealing at different temperatures (70, 110, 130 and 150 °C for 10 min).[45] The absorption enhancement seems to saturate at 110 °C after which increasing the annealing temperature has no positive effect on absorbance. Interestingly, annealing the films at 110 °C also gives the maximum photocurrent in the solar cells fabricated in the same study. Similar phenomena were also reported by Mihailetchi *et al.*[46] Chirvase *et al.*[38] demonstrated that the absorptions of pure RR-P3HT or PCBM show only slight changes whereas significant enhancement in the RR-P3HT absorption is observed in the blend films. In P3HT : PCBM 1 : 2 weight ratio films, the P3HT absorption was shown to increase continuously upon annealing at 130 °C for up to 70 minutes.

**4.1b. The improvement of crystallinity—X-ray diffraction.** The improved long-wavelength absorption of P3HT upon thermal annealing is only one part of the story. Due to the enhanced crystallinity of the polymer film, the hole mobility in P3HT also improves along with enhanced absorption. The improvement in hole mobility plays a significant role in device efficiency improvement, since the hole mobility of the P3HT donor is comparatively lower than the electron mobility of PCBM, which is recognized as a major bottleneck in device

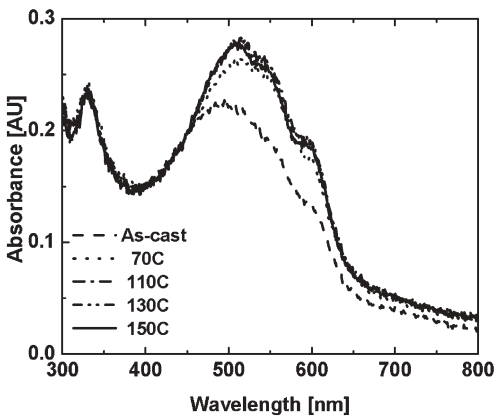


**Fig. 3** UV-Vis absorption spectra obtained for P3HT : PCBM thin films (80 nm, with PCBM conc. = 50 wt%) before and after annealing at different temperatures. The annealing time is 10 min for all the films. (Reprinted with permission from reference 45, copyright 2005, American Institute of Physics.)

 

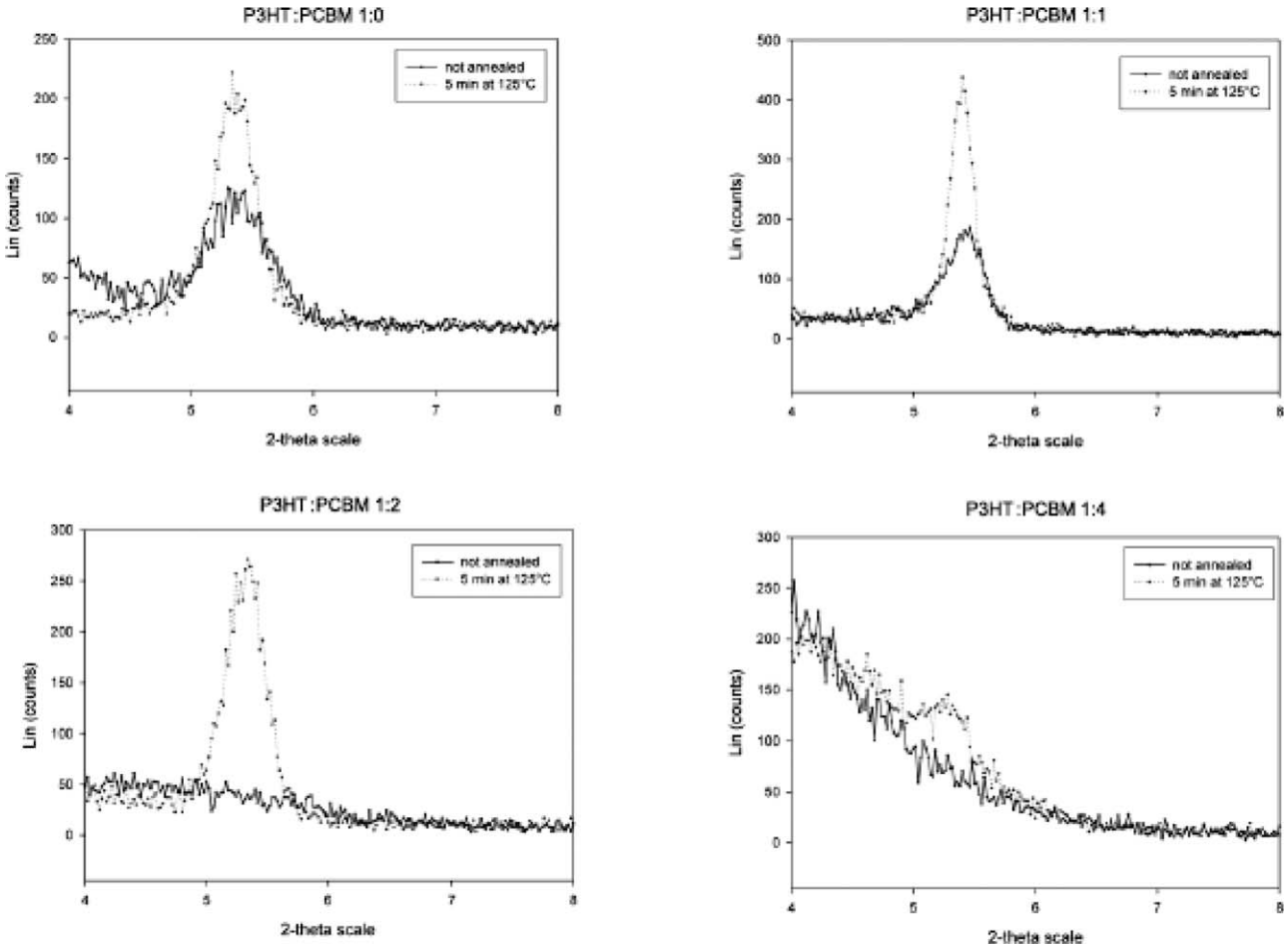


**Fig. 4** XRD of RR-P3HT : PCBM (1 : 0, 1 : 1, 1 : 2 and 1 : 4 weight ratio) films: as-cast *vs.* annealed at 125 °C for 5 min. (Reprinted with permission from reference 48, copyright 2007, EDP Sciences.)

performance. In the non-annealed blend films, the primary peaks are significantly diminished indicating significant reductions in polymer crystallinity. The crystallinity is clearly improved upon thermal annealing. Erb *et al.*[47] conducted an XRD study on as-cast and thermally annealed RR-P3HT : PCBM (1 : 2 weight ratio) films. After thermal annealing a single peak appeared corresponding to the polymer chain *a*-axis orientation (main chain parallel and side chains perpendicular to the substrate), with a layer spacing of 1.61 $\pm$ 0.2 nm. The mean size of the RR-P3HT crystallites was found to be about 8 nm. Swinnen *et al.* studied the XRD of non-annealed and annealed (125 °C, 5 min) RR-P3HT : PCBM blend films with different weight ratios (1 : 0, 1 : 1, 1 : 2 and 1 : 4; Fig. 4).[48] In addition to the common observation of enhanced crystallinity in all cases, it was observed that the ordering of RR-P3HT is hampered by the amount of PCBM, which agrees with the UV-Vis absorption spectra. Kim *et al.*[17d] also observed crystallization enhancement after annealing P3HT : PCBM blend films at 140 °C by GIXD measurements, as seen in Fig. 5.

**4.1c. The effect of composition.** Padinger *et al.*[43] reported 2.5% efficient solar cells using a RR-P3HT : PCBM 1 : 2 weight ratio active layer with relatively mild thermal annealing at 75 °C. Further electrical conditioning resulted in further improvement to 3.5% device efficiency. Several other groups,

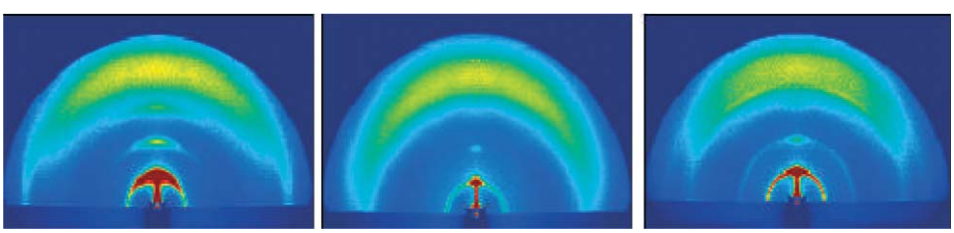

**Fig. 5** Two dimensional GIXRD images of (a) pristine RR-P3HT film, (b) non-annealed and (c) annealed (140 °C, 2 h) RR-P3HT : PCBM 1 : 1 films. (Reproduced with permission from reference 17(*d*), copyright 2006, Nature Publishing Group.)

however, found that thermal annealing at low temperature does not lead to significant polymer absorption enhancement. Instead, much lower PCBM loading (P3HT : PCBM in 1 : 1 or 1 : 0.8 weight ratio) compared to the optimized PPV derivative : PCBM system (1 : 4 weight ratio) was found to improve solar cell performance. In the MDMO-PPV : PCBM system higher PCBM loading is necessary since it results in a strong enhancement in hole mobility in the blend films.[49] The lower PCBM loading in the P3HT : PCBM active layer could be very beneficial to the long-term stability of polymer solar cells. Yang *et al.* have shown that thermal annealing of MDMO-PPV : PCBM 1 : 4 weight ratio films leads to highly accelerated phase segregation and formation of large PCBM single crystals due to thermally enhanced PCBM molecule diffusion mobility.[50] The long-term stability of the active layer is negatively affected in this case.

**4.1d. Morphology.** The BHJ structure basically consists of 3-D interpenetrating networks of donor and acceptor materials. The morphology of the polymer blend layer and the metal/polymer interface properties play important roles in determining device performance.[51,52] AFM images of the polymer film surface before and after annealing at different temperatures are shown in Fig. 6.[45] The surface of the as-cast film is very smooth with rms roughness ($\sigma_{rms}$) of 0.377 nm. After undergoing thermal treatment the $\sigma_{rms}$ first increases up to 110 °C and then decreases. The film texture also changes after annealing. The film annealed at 110 °C shows a much coarser texture with broad hill-like features compared to the other films. Higher film roughness gives higher device efficiency. However, the surface area of the roughest film is only about 0.1% more than that of a completely flat surface. Therefore the increased surface roughness probably does not play any direct role in efficiency improvement. Instead, higher surface roughness is more likely a signature of annealing enhanced ordered structure formation in the polymer film. Higher absorption and increase in the charge carrier mobility due to ordering are the most likely reasons for efficiency enhancement. An increase in surface roughness upon annealing was also observed independently by other groups.[17b,c]

In a TEM study on the effect of thermal annealing of the P3HT : PCBM system (Fig. 7), Yang *et al.*[53] reported that the P3HT crystals grow continuously into longer fibrils upon thermal annealing, as a signature of enhanced polymer crystallinity. Another important observation is the emergence of a segregated PCBM crystalline structure after thermal annealing, different from the uniform PCBM distribution in the as-cast film. The PCBM crystalline structure, however, does not grow into large size crystals as observed in MDMO-PPV : PCBM (1 : 4 weight ratio) films upon annealing.[50] Yang *et al.* suspected that growth of P3HT crystallites forms boundaries to hamper the extensive diffusion of PCBM molecules and their large-scale crystallization. This is especially helpful for the long term stability of these devices due to the formation of a stable film morphology upon thermal annealing. Indeed, the devices show relatively good stability under 70 °C for 1000 hour illumination.

Swinnen *et al.*[48] also observed the appearance of large crystalline PCBM structures (needles or fan-shaped) after annealing the blend films at high temperatures (*i.e.* 125–175 °C) for a short time (5 min) or at lower temperature (100 °C) for a few hours. The size of PCBM crystals grows as the PCBM loading increases or at higher annealing temperature. At 125 °C for 5 min, the needle size is several μm at 50 wt%

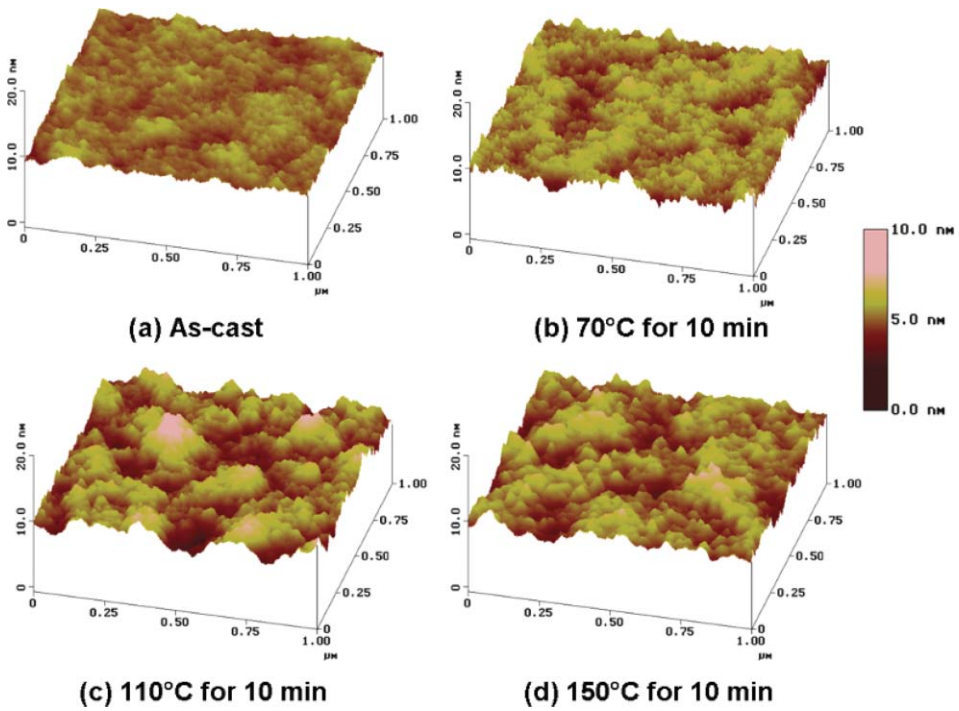


**Fig. 6** AFM height images of the P3HT : PCBM surface (a) before annealing, and after annealing at (b) 70 °C, (c) 110 °C, and (d) 150 °C for 10 min. (Reprinted with permission from reference 45, copyright 2005, American Institute of Physics.)

 

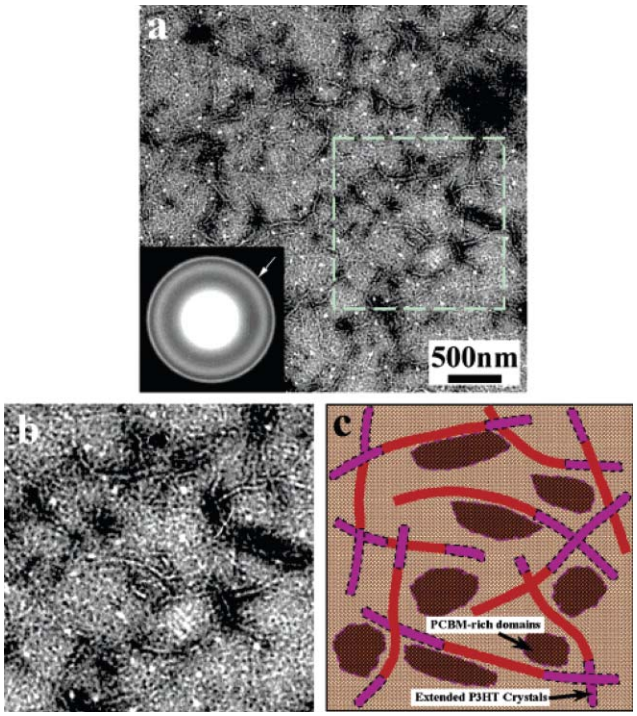


**Fig. 7** BF TEM images of the overview (a) and zoom in (b), and the corresponding schematic representation (c) of the thermal annealed RR-P3HT : PCBM active layer. (Reprinted with permission from reference 53, copyright 2005, ACS Publications.)

PCBM loading and the length is up to 100 μm at 80 wt% PCBM loading. These large sized PCBM structures degrade the film morphology and are obviously harmful for the device. It is consistent with the acceptance of low PCBM loading (~45 wt% PCBM) in several reports where a relatively high annealing temperature of 150 °C was found to be optimal for thermal annealing.[17b,c]

**4.1e. The effect on photoluminescence (PL)—improving phase separation and interpenetrating network of P3HT and PCBM.** Erb *et al.*[47] and Kim *et al.* (Fig. 8)[17d] have reported enhancement in PL of RR-P3HT in blend films upon thermal annealing, indicating the reduction of the interface area between the polymer and PCBM where the PL quenching occurs. These results are consistent with the improved polymer crystallization where more pure RR-P3HT and PCBM domains are formed. While this phase separation reduces exciton dissociation, the improved charge carrier transport in both donor and acceptor phases after thermal annealing offsets the former effect and results in an overall improvement in device performance.

**4.1f. The effect of active layer thickness.** The solar cell performance is also strongly affected by device thickness. Fig. 9 shows $J_{SC}$ and PCE of P3HT : PCBM solar cells with different active layer thicknesses after post-production treatment at 110 °C for 10 minutes. The oscillatory behavior of $I_{SC}$ as a function of thickness could be due to: (a) optical effects, and, (b) low charge carrier mobility. PCE of 4.0% is achieved for the device with thickness $t$ = 63 nm. It is clear that the

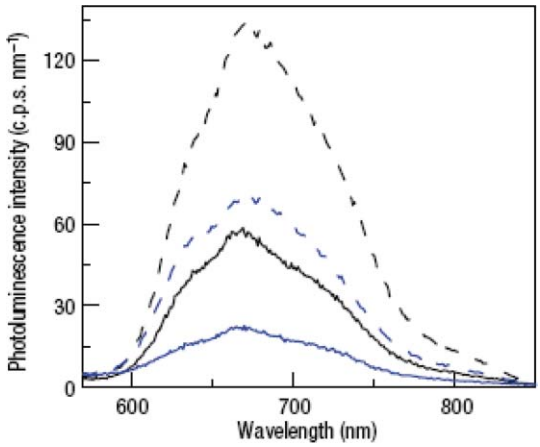


**Fig. 8** Photoluminescence spectra of P3HT : PCBM (1 : 1 weight ratio) films (~200 nm thick): black 95.2% RR, blue 90.7 RR; solid and dashed lines denote not-annealed and annealed (140 °C, 2 h) respectively. (Reproduced with permission from reference 17(*d*), copyright 2006, Nature Publishing Group.)

efficiency can be increased by more than twice if an optimum thickness of active layer is used. The fact that a thicker device does not give the best performance indicates that the charge carrier mobility is still a limiting factor in this type of solar cell even after thermal annealing.

### 4.2. Solvent annealing (slow growth)

To achieve a highly efficient PV device, solar radiation needs to be efficiently absorbed and the charge transport must be efficient following the charge separation at the D/A interface. In the RR-P3HT system, the enhanced crystallinity of the polymer will enhance both the absorption in the long wavelength range and the hole mobility. However, only a partial recovery of the RR-P3HT absorption in the blend film after thermal annealing suggests that this approach is not sufficient to fully exploit the potential of the RR-P3HT : PCBM system.

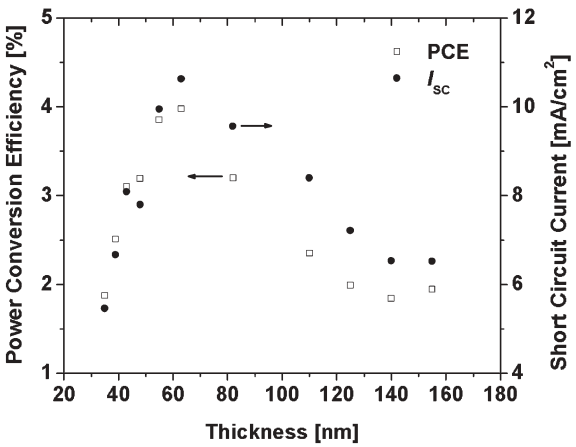


**Fig. 9** Short circuit current density ($J_{SC}$) and power conversion efficiency (PCE) as a function of active layer thickness. Devices were annealed at 110 °C for 10 min post-production. (Reprinted with permission from reference 45, copyright 2005, American Institute of Physics.)

Additional evidence is the fact that a thicker film does not lead to a more efficient device, indicating the existence of the carrier transport bottleneck. These limitations can be overcome through another approach called "solvent annealing" (or slow growth). Instead of recovering the RR-P3HT crystallinity (ordering) which is lost during the fast solvent removing (fast spin-coating) process, this approach aims at maintaining the polymer ordering during the film formation stage. Reducing the solvent removal speed results in self-organization in polymer chains by controlling the active polymer layer growth rate from solution to the solid state. The intrinsic polymer self-organization capability gives higher absorption, higher carrier mobility, and balanced carrier transport. In the following sections we will discuss the effects of solvent annealing, or slow growth, on absorption, polymer film morphology, charge carrier mobility, and exciton generation and dissociation in the active layer.

**4.2a. Effect of solvent annealing on absorption.** The UV-Vis absorption spectra of slow- and fast-grown films are shown in Fig. 10, before and after thermal annealing at 110 °C for 20 min.[17a] High boiling point solvent and low spin speed were chosen and the films were in the liquid phase after spin-coating. The films formed by slowly removing the solvent in a covered glass Petri dish are referred to as slow-grown films, while the fast removal of solvent by heating the spin-cast film at 70 °C gives fast-grown films. The absorption in the red region for the slow-grown film is significantly stronger compared to that of the fast-grown film. The three vibronic absorption features are the most prominent reported in the literature, indicating strong interchain–interlayer interactions[34–36] of RR-P3HT chains, as well as well-maintained polymer ordering in the blend films. After annealing at 110 °C for 20 min, the absorbance of the fast-grown film shows a significant increase and the vibronic features become clearer, indicating a partial recovery of ordering. For the slow-grown film, the absorption spectra show no significant differences before and after thermal annealing, further strengthening the argument that the slow-grown film already has a high degree of ordering. The absorption of the slow-grown film is a simple addition of the absorption of the two components in the film, which strongly supports the occurrence of phase segregation and the formation of crystalline RR-P3HT domains in the blend film. PCBM absorption is clearly unaffected by the solvent removing speed, which indicates that the driving force of device improvement is self-organization of the polymer through the solvent annealing process. This also agrees with the observation by Swinnen *et al.* that the crystal formation process in PCBM is much slower than that in RR-P3HT.[48]

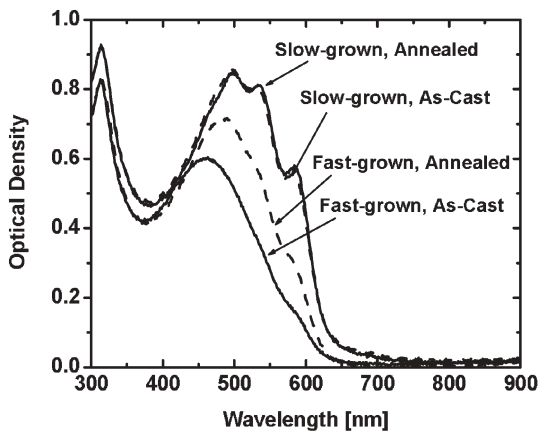


**Fig. 10** UV-Vis absorption spectra for slow- and fast-grown P3HT : PCBM films, before and after thermal annealing at 110 °C for 20 minutes. (Reproduced with permission from reference 17(*a*), copyright 2005, Nature Publishing Group.)

**4.2b. Effect of solvent annealing on morphology.** The AFM height and phase images (Fig. 11) show that the slow-grown film (a) has $\sigma_{RMS} \sim 9.5$ nm, whereas the fast-grown film (b) has a very smooth surface with $\sigma_{RMS} \sim 0.87$ nm. The rough surface of the slow-grown film is most likely a signature of polymer (blend) self-organization which in turn enhances ordered structure formation in the film. The peak to valley height of the slow grown film is about 100 nm, corresponding to 50% of the mean thickness (210 nm). The phase image of the fast-grown film (d) shows coarse chain-like (fibrillar) features running across the surface. These fibrillar features are assigned to the domains of pure P3HT crystallites. The region between these features is a disorder zone which harbors structural defects like chain ends and folds as wells as tie segments.[54] PCBM molecules suppress the formation of P3HT crystallites in the fast-grown films and most of the film consists of mixed domains which are amorphous in nature. For the slow-grown film (c), the crystalline domains of pure P3HT chains are denser. They have a strong tendency to form an interconnecting network and are distributed more uniformly throughout the film. The separation distance between the features is also less, which suggests tighter packing of P3HT crystallites in the slow-grown film. The separation distance between surface features in the slow-grown film ($\sim$28 nm) is smaller than that in the fast-grown film ($\sim$55 nm). The crystallite size estimated from AFM phase images matches the results from XRD data on similar films,[47] where the mean crystallite size estimated from Scherrer's equation is 10–50 nm. The reduced crystallite size and inter-crystallite spacing are believed to be the results of higher ordering. P3HT chains get more time to self-organize into a more ordered structure during very slow growth. As a result, the regions of mixed P3HT/PCBM domains will reduce.

The overall crystalline structure of RR-P3HT in the solvent annealed RR-P3HT : PCBM 1 : 1 weight ratio blend films has been studied with the aid of GIXD analysis using the synchrotron source in Brookhaven National Lab.[55] 2D GIXD patterns of the solvent annealed blend film clearly show the intense reflections of the (100) layer and (010) crystals along the $q_z$ (substrate normal) and $q_{xy}$ (substrate parallel) axis, respectively, implying that the films have highly ordered edge-on hexyl side chains and parallel π-conjugated planes of RR-P3HT with respect to the substrate (the same as in pure P3HT films).[56,57] The GIXD peaks are very strong, indicating superior crystallinity obtained in this approach. The highly crystalline blend film showed an inter-layer spacing of 16.1 Å.

**4.2c. *I–V* characteristics.** In Fig. 12a, $I_{sc}$ reduces from 9.9 mA cm$^{-2}$ in a device with a slow-grown highly ordered

 

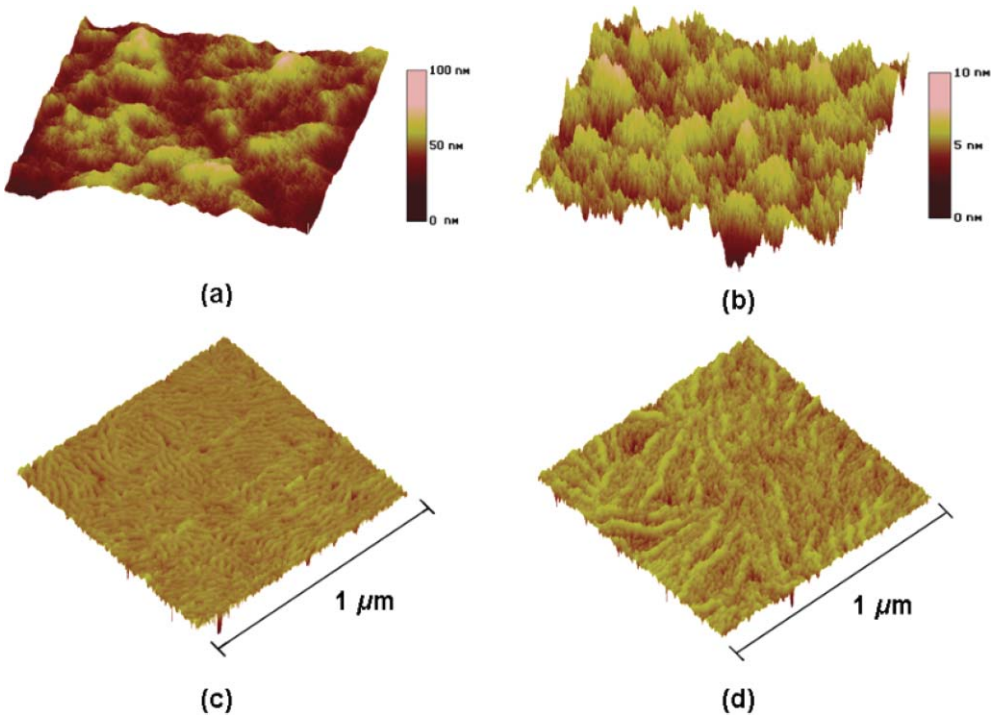


**Fig. 11** AFM images for different growth rate of polymer active layer. Height images for (a) slow- and (b) fast-grown films. Phase images for (c) slow- and (d) fast-grown films. (Reproduced with permission from reference 17(*a*), copyright 2005, Nature Publishing Group.)

active layer to 4.5 mA $cm^{-2}$ in that with a fast-grown active layer, showing the effect of the solvent annealing approach. The device series resistance, $R_{SA}$, increases from 2.4 to 19.8 $\Omega.cm^2$, with increasing film growth rate. The fill factor (FF) also decreases from 60.3% to 52.0%. The low $R_{SA}$ of 2.4 $\Omega$ $cm^2$ (for the slow-grown device) is comparable to those of much thinner devices ($\sim$48 nm),[45] underlining the effect of self-organization.

Although solvent annealed films consist of highly ordered polymer chains, which cannot be achieved through thermal annealing, the extra step of annealing the films provides further enhancement in device performance due to different effects. The *I–V* curves under illumination for four devices with annealing (at 110 °C) times ($t_A$) are shown in Fig. 12b. All four devices were made from blend films which were slow-grown. Upon annealing, $I_{SC}$ increases slightly from 9.9 to 10.6 mA $cm^{-2}$, FF increases from 60.3% to 67.4%, and the PCE improves from 3.5% to 4.4%. Under dark conditions, the rectification ratios are close to $10^7$ at a bias of 2 V. The reason behind the high FF in slow-grown devices is believed to be the significantly large thickness of the active layer. The thickness of the active layer makes it free of pinholes and microcracks and all devices show very high shunt resistance in the range of 180–640 MΩ as derived from the *I–V* characteristics measured in the dark. The ultrahigh shunt resistance reduces the noise equivalent power (NEP) of the device and makes it ideal for photo-detector applications. Moreover, the surface of the active layer becomes smoother upon annealing which enables a very good, defect-free contact with the metal cathode, thereby increasing the FF values.

The EQE for the device with a fast-grown film shows a maximum of $\sim$19% at a wavelength of 350 nm. On the other hand, for the device with a slow-grown film, the EQE maximum increases by more than three times to $\sim$63% at 500 nm (Fig. 13). This increase in EQE over the wavelength range of 350–650 nm contributes to the increase in the power conversion efficiency of the devices. The enhancement in EQE clearly originates from two important contributions: an increase in the charge carrier mobility and increased absorption in the active layer.

**4.2d. Effect of solvent annealing on charge carrier mobility.** Time-of-flight (TOF) study conducted on slow- and fast-grown films at $E \sim 2 \times 10^5$ V $cm^{-1}$ shows that in the slow-grown film both electron and hole transport is non-dispersive with $\mu_e = 7.7 \times 10^{-5}$ and $\mu_h = 5.1 \times 10^{-5}$ $cm^2$ $V^{-1}$ $s^{-1}$, whereas for the fast-grown film dispersive hole transport and a significant reduction in $\mu_h$ to $5.1 \times 10^{-6}$ $cm^2$ $V^{-1}$ $s^{-1}$ are observed. The electron mobility increases slightly to $1.1 \times 10^{-4}$ $cm^2$ $V^{-1}$ $s^{-1}$. The destruction of the ordered structure during fast growth is believed to be the reason for this. In addition, in the slow-grown film the ratio between electron and hole mobilities is close to unity ($\mu_e/\mu_h \sim 1.5$) resulting in balanced carrier transport in the active layer (Fig. 14).[17*a*,58]

The electron and hole mobilities are also measured by fitting the dark *J–V* curves for single carrier devices to the space-charge limited current (SCLC) model at low voltages, where the current is given by $J = 9\varepsilon_0\varepsilon_r\mu V^2/8L^3$, where $\varepsilon_0\varepsilon_r$ is the permittivity of the polymer, $\mu$ is the carrier mobility and $L$ is the device thickness.[59] The hole-only devices using high work function ($\Phi_F$) metal oxide $MoO_3$ ($\Phi_F$ = 5.3 eV) to replace Ca, and electron-only devices with low work function $Cs_2CO_3$ to replace PEDOT : PSS in the regular solar cell structure, are tested with the active layer of P3HT/PCBM obtained by slow

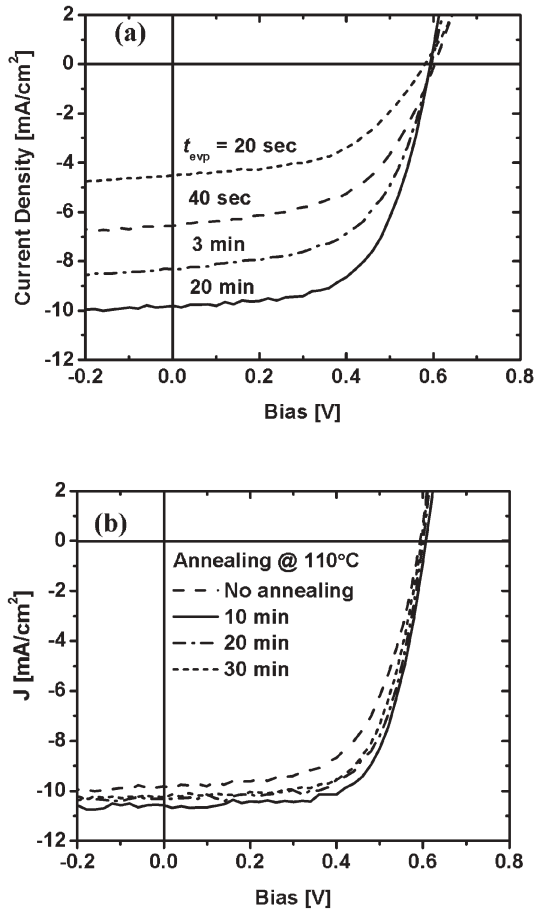


**Fig. 12** (a) *I–V* characteristics under illumination for devices with different film growth rates by varying the solvent evaporation time, $t_{evp}$. (b) *I–V* curves for devices with an active layer before and after thermal annealing at 110 °C for 10, 20, and 30 min. The active layer thickness was 210 nm and the film growth time was $t_{evp} \sim 20$ minutes. (Reproduced with permission from reference 17(*a*), copyright 2005, Nature Publishing Group.)

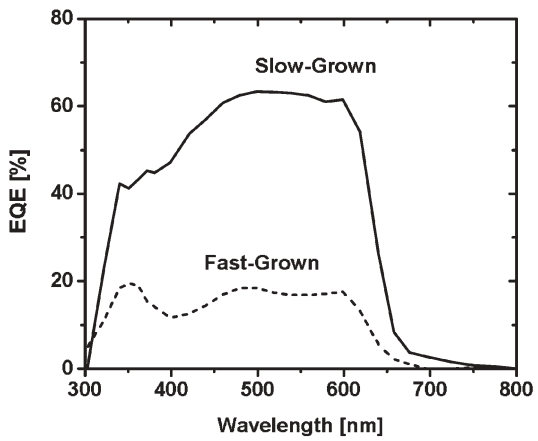


**Fig. 13** EQE for P3HT : PCBM solar cells for two types of active layers: slow-grown and fast-grown. The efficiency maximum for the slow-grown film is ~63% which is more than three times that of the fast-grown film (~19%). (Reproduced with permission from reference 17(*a*), copyright 2005, Nature Publishing Group.)

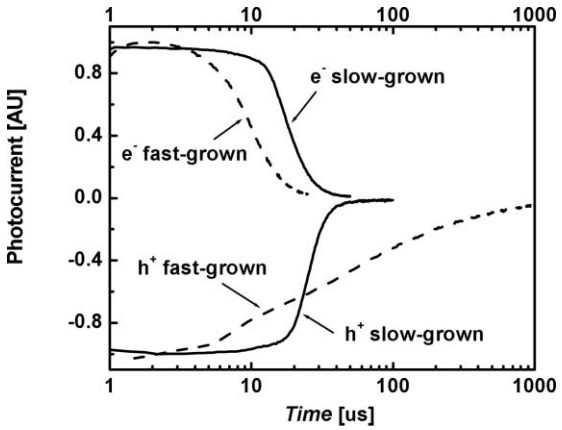


**Fig. 14** Time of flight (TOF) signals of slow- and fast-grown films plotted on a semi-log scale. Films were prepared in the same way as cells in this study with film thickness of about 1 μm. (Reproduced with permission from reference 17(*a*), copyright 2005, Nature Publishing Group.)

and fast growth. For the fast-grown films the mobilities are $\mu_e \sim 6.5 \times 10^{-8}$ and $\mu_h \sim 1.9 \times 10^{-9}$ m$^2$ V$^{-1}$ s$^{-1}$. For the slow-grown film the electron mobility increases by four times to $2.6 \times 10^{-7}$ m$^2$ V$^{-1}$ s$^{-1}$, and the hole mobility increases by about two orders of magnitude to $1.7 \times 10^{-7}$ m$^2$ V$^{-1}$ s$^{-1}$. The ratio of electron to hole mobility is about 1.5 (Fig. 15). Independently, Mihailetchi *et al.* also reported a similar study on a device with a slow-grown active layer with no further thermal annealing.[60] A hole mobility of $5.0 \times 10^{-7}$ m$^2$ V$^{-1}$ s$^{-1}$

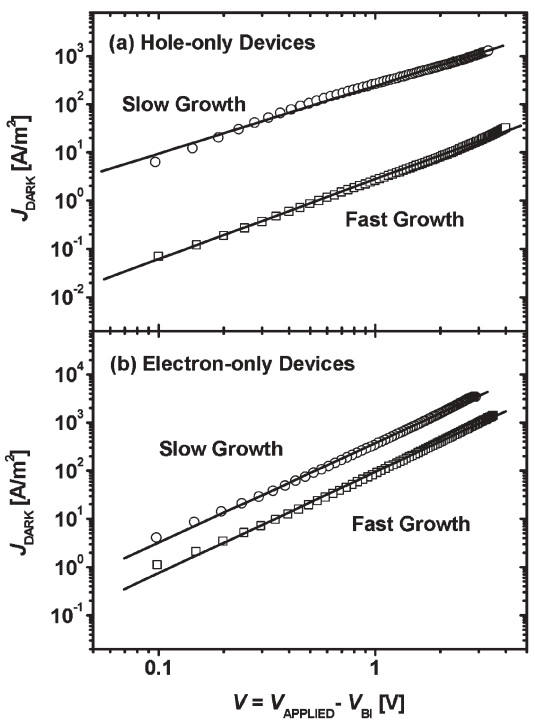


**Fig. 15** *J–V* curves in the dark for (a) hole-only and (b) electron-only device for different growth rates. The solid lines represent the fit to the experimental data using SCLC model. (Reprinted with permission from reference 59, copyright 2006, American Institute of Physics.)

 

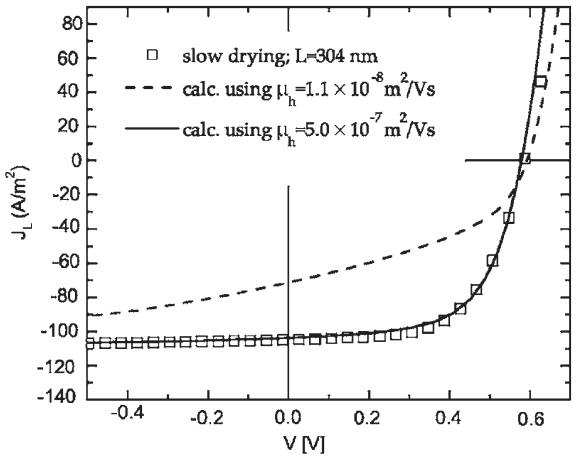


**Fig. 16** Experimental data of a RR-P3HT : PCBM blend solar cell device prepared by the slow-growth method of active layer (squares), together with the model calculation, using the hole mobility measured in the fast-drying film (dashed line) and slow-drying film (solid line). (Reprinted with permission from reference 60, copyright 2006, American Institute of Physics.)

was derived from the model (Fig. 16). This value represents a 33-fold increase of the RR-P3HT hole mobility compared to the device with optimized thermal annealing only.[61] The high hole mobility leads to balanced electron and hole transport, and reduced space-charge accumulation. An active layer thickness over 300 nm does not lower the device fill factor and photocurrent. The superior performance of the device with a slow-grown active layer over the thermally annealed device is attributed to the improved absorption of incoming photons.

**4.2e. Exciton generation and dissociation.** The effect of solvent annealing on photocurrent generation in the device has been studied by examining *I–V* curves measured in reverse bias under 100 mW cm$^{-2}$ simulated AM1.5G conditions using method adopted by Mihailetchi *et al.*[62,63] for the MDMO-PPV/PCBM system. At large reverse bias ($V_{EFF} = V_0 - V >$ 10 V), photocurrent ($J_{PH}$) saturates for both devices with a saturation photocurrent ($J_{SAT}$) of ~125 A m$^{-2}$ for the fast- and ~155 A m$^{-2}$ for the slow-grown film. The maximum generation rate ($G_{max}$; given as $J_{SAT} = eG_{max}L$) is 3.5 × 10$^{27}$ m$^{-3}$ s$^{-1}$ and 4.4 × 10$^{27}$ m$^{-3}$ s$^{-1}$ for the fast- and slow-grown films, respectively, for film thickness $L$ = 220 nm (Fig. 17). Upon changing the growth rate of the film from fast to slow, the electron–hole pair generation in the film increases by about 26%, which is attributed to the increased absorption in the slow-grown film as discussed earlier.

Onsager's theory of ion-pair dissociation in weak electrolytes,[64] later modified by Braun,[65] was used in the system. In the fast-grown film, at the short-circuit condition ($V_{EFF} = V_0$) only 57% of the total photo-generated electron–hole pairs dissociate into free carriers, which further reduces to 41% at the maximum power output point ($V$ = 0.4 V). This suggests that more than half of the generated electron–hole pairs are lost due to recombination in fast-grown films. On the other hand, the electron–hole pair dissociation efficiency of the device with the slow-grown film is more than 80% at the

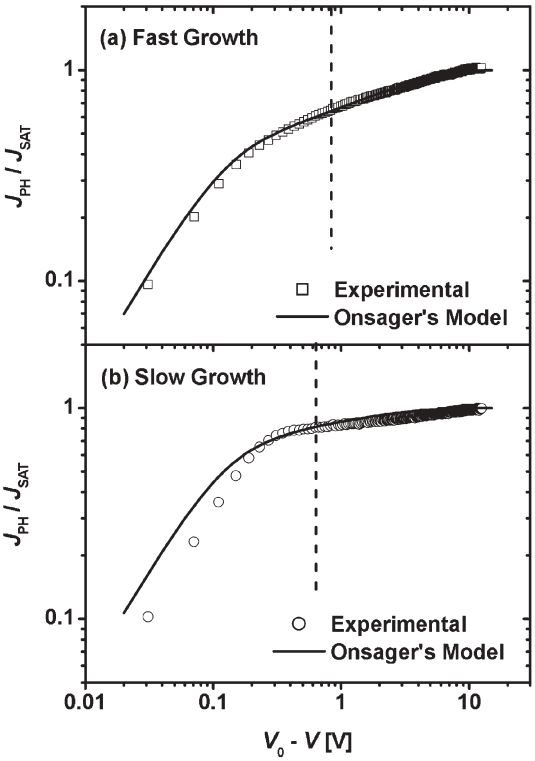


**Fig. 17** Measured (open symbols) and calculated (solid curves) normalized photocurrent as a function of effective applied bias for (a) fast- and (b) slow-grown films. (Reprinted with permission from reference 59, copyright 2006, American Institute of Physics.)

short-circuit condition. At the maximum power output bias, the dissociation efficiency is still around 70%. Such high dissociation efficiency values clearly demonstrate the effect of self-organization induced ordering in the blend films.

### 4.3. Regioregularity and molecular weight effect

In addition to the active layer tempering, regularity of the polymer and molecular weight are also shown to play important roles in the solar cell performance. Kim *et al.* studied the effect of the degree of regioregularity (RR) on the performance of polymer solar cells with P3HT : PCBM 1 : 1 weight ratio.[17d] The absorption coefficient is observed to increase with increasing RR, particularly on the longest wavelength shoulder formed by polymer inter-chain interactions. In the resulting solar cell, both $J_{SC}$ and EQE have positive correlations with RR. This correlation is well preserved upon thermal annealing. The combination of increased absorption and charge transport (as the result of more organized polymer chain packing) again explains the performance improvement.

Another important parameter which strongly affects the device performance is the molecular weight (MW) of the P3HT polymer. Kline *et al.*[66] and Zen *et al.*[67] studied the hole mobility of RR-P3HT with different MWs (by controlling synthesis route, polymerization time, and fractionated solvents with different solvency) in field-effect transistors. Kline *et al.* found that although low MW RR-P3HT has higher crystalline order, the field-effect mobility is higher when MW is larger. The

mobility steadily increases with MW from $1.7 \times 10^{-6}$ $cm^2$ $V^{-1}$ $s^{-1}$ in a 3.2 kDa MW device to $9.4 \times 10^{-3}$ $cm^2$ $V^{-1}$ $s^{-1}$ in a 36.5 kDa MW device. The results are explained by the fact that the charge carriers in RR-P3HT delocalize over several neighboring chains.[68,69] High MW P3HT fractions have a planar π-stacked conformation while the low MW fractions have a more twisted, disordered inter-chain conformation. Films from the high MW fractions have absorption spectra with well-resolved vibrational structure, which is missing in those from low MW fractions. The same trend is observed in the absorption of RR-P3HT : PCBM films with different MWs.[70] The photovoltaic test shows that high molecular weight leads to solar cells with 10–20 fold efficiency enhancement compared to those using low molecular weight fractions, and only the RR-P3HT with a number-average molecular weight ($M_n$) $>$ 10 000 gives high power conversion efficiency.

## 5. Future directions and challenges

The further improvement of polymer solar cells requires research on new polymers with band-gaps lower than those of current state-of-the-art RR-P3HT.[71] The absorption edge of a RR-P3HT : PCBM film is around 650 nm and extending the band-gap of the polymer to 900 nm or beyond will increase the photon absorption in the active layer by 100% or more. To improve the efficiency, the energy level offset between the donor polymer and the acceptor has to be minimized while still allowing sufficient energy offset for efficient exciton dissociation. Finally, polymers with high hole mobility values are desired. Scharber *et al.*[72] and Koster *et al.*[73] have independently modeled the energy-conversion efficiency *versus* band-gap and LUMO level of the donor polymer, and HOMO level of the acceptor. By assuming the high fill factor achieved in the RR-P3HT : PCBM system, a single layer polymer solar cell with efficiency over 10% under standard reporting conditions (SRC) is predicted. The challenge is how to realize a polymer with all the preferred properties. Although synthetic principles for band-gap control in linear π-conjugated system[74] has been established and several promising low bandgap polymer : PCBM systems have been reported,[75] the performance of solar cells based on these systems still remains lower compared to the best RR-P3HT : PCBM solar cells. For example, a polymer promising to achieve 7% efficiency with its preferred energy levels shows only 3.2% efficiency.[75d]

Efficient light harvesting can be achieved by using a tandem cell (each covering a different solar spectrum region) structure in small molecular organic solar cells by thermal evaporation.[76] In polymer solar cells, the damage to the bottom cell due to solution processing involved in device fabrication is a severe problem. Very recently, Janssen *et al.* successfully demonstrated double- and triple-junction solution process polymer solar cells.[77] The combination of spin-coating ZnO nanoparticles and neutral pH PEDOT leads to a $V_{oc}$ of the multiple junction solar cells (2.19 V for a triple junction device) close to the $V_{oc}$ summation of the individual cells, indicating the effectiveness of this approach. An alternative way to achieve a tandem cell structure in polymer solar cells is multiple-device stacking.[78] This approach decouples the fabrication of the two cells. The freedom of interconnection is intrinsic and it also increases the yield of production. The challenges include (a) development of transparent electrodes for high efficiency solar cells; (b) the additional substrate/air interface which leads to additional photon loss, and (3) proper material systems with efficient absorption in different solar spectral ranges. Recently, an inverted device structure was proposed to realize transparent solar cells.[79]

The "ordered bulk-heterojunction" concept[80] has been proposed to improve the charge transport problem. In such a structure, each photogenerated exciton is within a diffusion length of the electron acceptor, and both polymer and acceptor have straight pathways to the electrodes to reduce carrier recombination and increase charge collection efficiency. The efficiency of these ordered BHJ cells is currently low, but this approach is among the more promising approaches to realize high efficiency polymer solar cells. The challenges include the formation of nanostructure pore sizes comparable to the exciton diffusion length and filling the polymer chains into these pores.

Finally, the stability of polymer solar cells must be addressed for this technology to be commercialized. This involves both materials improvement and development of highly effective encapsulation schemes.

## Acknowledgements

The authors are grateful for the financial support provided by the Office of Naval Research (ONR) (Grant number N00014-04-1-0434), Solarmer Energy Inc., University of California Discovery Grant, and the Nanoscale Science and Engineering Institute of the National Science Foundation (NSF) (Grant number DMR 0117792).

## References

1 (*a*) J. A. Turner, *Science*, 1999, **285**, 687; (*b*) M. I. Hoffert, K. Caldeira, G. Benford, D. R. Criswell, C. Green, H. Herzog, A. K. Jain, H. S. Kheshgi, K. S. Lackner, J. S. Lewis, H. D. Lightfoot, W. Manheimer, J. C. Mankins, M. E. Mauel, L. J. Perkins, M. E. Schlesinger, T. Volk and T. M. L. Wigley, *Science*, 2002, **298**, 981.
2 (*a*) http://www.sc.doe.gov/bes/reports/files/SEU_rpt.pdf, Report of the Basic Energy Sciences Workshop on Solar Energy Utilization", US-DOE, April 18–21, 2005; (*b*) Energy Information Administration, U.S. Department of Energy, Overview, Annual Energy Outlook 2003.
3 C. Fritts, *Proc. Am. Assoc. Adv. Sci.*, 1883, **33**, 97.
4 D. Chapin, C. Fuller and G. Pearson, *J. Appl. Phys.*, 1954, **25**, 676.
5 S. Hegedus and A. Luque, in *Handbook of photovoltaics science and engineering*, ed. A. Luque and S. Hegedus, Wiley, West Sussex, 2003, p. 1.
6 R. C. Armstrong and E. J. Moniz, *Report of the energy research council*, Massachusetts Institute of Technology, Cambridge, MA, 2006.
7 C. K. Chiang, C. R. Fincher, Y. W. Park, A. J. Heeger, H. Shirakawa, E. J. Louis, S. C. Gua and A. G. MacDiarmid, *Phys. Rev. Lett.*, 1977, **39**, 1098; W. P. Su, J. R. Schrieffer and A. J. Heeger, *Phys. Rev. Lett.*, 1979, **42**, 1698.
8 C. W. Tang and S. VanSlyke, *Appl. Phys. Lett.*, 1986, **51**, 913.
9 J. H. Burroughes, D. D. C. Bradley, A. R. Brown, R. N. Marks, K. Mackay, R. H. Friend, P. L. Burns and A. B. Holmes, *Nature*, 1990, **347**, 539; R. H. Friend, R. W. Gymer, A. B. Holmes, J. H. Burroughes, R. N. Marks, C. Taliani, D. D. C. Bradley, D. A. Dos Santos, J. L. Brédas, M. Lögdlund and W. R. Salaneck, *Nature*, 1999, **397**, 121.

 

10 G. Horowitz, X. Z. Peng, D. Fichou and F. Garnier, *Solid State Commun.*, 1989, **72**, 381.
11 H. Sirringhaus, P. J. Brown, R. H. Friend, M. M. Nielsen, K. Bechgaard, B. M. W. Langeveld-Voss, A. J. H. Spiering, R. A. J. Janssen, E. W. Meijer, P. Herwig and D. M. de Leeuw, *Nature*, 1999, **401**, 685.
12 Z. Bao, A. Dodabalapur and A. J. Lovinger, *Appl. Phys. Lett.*, 1995, **69**, 4108.
13 L. Ma, J. Liu and Y. Yang, *Appl. Phys. Lett.*, 2002, **80**, 2997.
14 L. Ma, S. Pyo, J. Ouyang, Q. Xu and Y. Yang, *Appl. Phys. Lett.*, 2003, **82**, 1419.
15 S.-S. Sun and N. S. Sariciftci, *Organic photovoltaics: mechanisms, materials, and devices*, CRC Press, Boca Raton, FL, 2005.
16 C. J. Brabec, V. Dyakonov, J. Parisi and N. S. Sariciftci, *Organic photovoltaics: concepts and realization*, Springer, Berlin, Germany, 2003.
17 (*a*) G. Li, V. Shrotriya, J. Huang, Y. Yao, T. Moriarty, K. Emery and Y. Yang, *Nat. Mater.*, 2005, **4**, 864; (*b*) W. Ma, C. Yang, X. Gong, K. Lee and A. J. Heeger, *Adv. Funct. Mater.*, 2005, **15**, 1617; (*c*) M. Reyes-Reyes, K. Kim and D. L. Carroll, *Appl. Phys. Lett.*, 2005, **87**, 083506; (*d*) Y. Kim, S. Cook, S. M. Tuladhar, S. A. Choulis, J. Nelson, J. R. Durrant, D. D. C. Bradley, M. Giles, I. McCulloch, C.-S. Ha and M. Ree, *Nat. Mater.*, 2006, **5**, 197.
18 M. C. Scharber, D. Mühlbacher, M. Koppe, P. Denk, C. Waldauf, A. J. Heeger and C. J. Brabec, *Adv. Mater.*, 2006, **18**, 789.
19 N.-K. Persson and O. Inganas, in *Organic photovoltaics: mechanisms, materials, and devices*, ed. S.-S. Sun and N. S. Sariciftci, CRC Press, Boca Raton, FL, 2005, p. 107.
20 P. Peumans, A. Yakimov and S. R. Forrest, *J. Appl. Phys.*, 2003, **93**, 3693.
21 C. J. Brabec, A. Cravino, D. Meissner, N. S. Sariciftci, T. Fromherz, M. T. Rispens, L. Sanchez and J. C. Hummelen, *Adv. Funct. Mater.*, 2001, **11**, 374.
22 M. Pope and C. E. Swenberg, *Electronic processes in organic crystals*, Clarendon Press, Oxford, 1982.
23 H. S. Nalwa, *Handbook of organic conductive molecules and polymers*, (Wiley, New York, 1997, vol. 1–4.
24 N. S. Sariciftci, L. Smilowitz, A. J. Heeger and F. Wudl, *Science*, 1992, **258**, 1474.
25 C. J. Brabec, G. Zerza, N. S. Sariciftci, G. Cerullo, S. DeSilvestri, S. Luzatti and J. C. Hummelen, *Chem. Phys. Lett.*, 2001, **340**, 232.
26 G. Yu, J. Gao, J. C. Hummelen, F. Wudl and A. J. Heeger, *Science*, 1995, **270**, 178.
27 J. J. M. Halls, C. A. Walsh, N. C. Greenham, E. A. Marseglia, R. H. Friend, S. C. Moratti and A. B. Holmes, *Nature*, 1995, **376**, 498.
28 K. Emery and C. Osterwald, *Current topics in photovoltaics*, Academic Press, London, 1988; K. Emery and C. Osterwald, *Sol. Cells*, 1986, **17**, 253; K. Emery, in *Handbook of photovoltaic science and engineering*, ed. A. Luque and S. Hegedus, Wiley, West Sussex, UK, 2003.
29 V. Shrotriya, G. Li, Y. Yao, Y. Yang, T. Moriarty and K. Emery, *Adv. Funct. Mater.*, 2006, **16**, 2016.
30 K. Emery, C. Osterwald, T. W. Cannon, D. R. Myers, J. Burdick, T. Glatfelter, W. Czubatyj and J. Yang, in *Proc. 18th IEEE Photovoltaic Specialist Conf.*, 1985, IEEE, New York, p. 623; C. Osterwald, *Sol. Cells*, 1986, **18**, 269.
31 S. E. Shaheen, C. J. Brabec, F. Padinger, T. Fromherz, J. C. Hummelen and N. S. Sariciftci, *Appl. Phys. Lett.*, 2001, **78**, 841.
32 M. M. Wienk, J. M. Kroon, W. J. H. Verhees, J. Knool, J. C. Hummelen, P. A. van Hal and R. A. J. Janssen, *Angew. Chem., Int. Ed.*, 2003, **42**, 3371.
33 H. Hoppe and N. S. Sariciftci, *J. Mater. Chem.*, 2006, **16**, 45.
34 (*a*) R. D. McCullough, S. Tristram-Nagle, S. P. Williams, R. D. Lowe and M. Jayaraman, *J. Am. Chem. Soc.*, 1993, **115**, 4910; (*b*) T.-A. Chen, X. Wu and R. D. Rieke, *J. Am. Chem. Soc.*, 1995, **117**, 233.
35 H. Sirringhaus, N. Tessler and R. H. Friend, *Science*, 1998, **280**, 1741.
36 P. J. Brown, D. S. Thomas, A. Kohler, J. S. Wilson, J.-S. Kim, C. M. Ramsdale, H. Sirringhaus and R. Friend, *Phys. Rev. B*, 2003, **67**, 064203.
37 V. Shrotriya, J. Ouyang, R. J. Tseng, G. Li and Y. Yang, *Chem. Phys. Lett.*, 2005, **411**, 138.
38 D. Chirvase, J. Parisi, J. C. Hummelen and V. Dyakonov, *Nanotechnology*, 2004, **15**, 1317.
39 M. Berggren, G. Gustafsson, O. Inganas, M. R. Andersson, O. Wennerstrom and T. Hjerberg, *Appl. Phys. Lett.*, 1994, **65**, 1489.
40 Y. Zhao, G. X. Yuan, P. Roche and M. Leclerc, *Polymer*, 1995, **36**, 2211.
41 N. Camaioni, G. Ridolfi, G. Casalbore-Miceli, G. Possamai and M. Maggini, *Adv. Mater.*, 2002, **14**, 1735.
42 J. J. Dittmer, E. A. Marseglia and R. H. Friend, *Adv. Mater.*, 2000, **12**, 1270.
43 F. Padinger, R. S. Rittberger and N. S. Sariciftci, *Adv. Funct. Mater.*, 2003, **13**, 85.
44 Y. Kim, S. A. Choulis, J. Nelson, D. D. C. Bradley, S. Cook and J. R. Durrant, *Appl. Phys. Lett.*, 2005, **80**, 3885.
45 G. Li, V. Shrotriya, Y. Yao and Y. Yang, *J. Appl. Phys.*, 2005, **98**, 043704.
46 V. D. Mihailetchi, H. Xie, B. de Boer, L. J. A. Koster and P. W. M. Blom, *Adv. Funct. Mater.*, 2006, **16**, 699.
47 T. Erb, U. Zhokhavets, G. Gobsch, R. Raleva, B. Stuhn, P. Schilinsky, C. Waldauf and C. J. Brabec, *Adv. Funct. Mater.*, 2005, **15**, 1193.
48 A. Swinnen, I. Haeldermans, P. Vanlaeke, J. D'Haen, J. Poortmans, M. D. 'Olieslaeger and J. V. Manca, *Eur. Phys. J.: Appl. Phys.*, 2007, **36**, 251.
49 C. Melzer, E. J. Koop, V. D. Mihailetchi and P. W. M. Blom, *Adv. Funct. Mater.*, 2004, **14**, 865.
50 X. Yang, J. K. J. Van Duren, R. A. J. Janssen, M. A. J. Michels and J. Loos, *Macromolecules*, 2004, **37**, 2151.
51 J. Liu, Y. Shi and Y. Yang, *Adv. Funct. Mater.*, 2001, **11**, 420.
52 H. Hoppe, M. Niggemann, C. Winder, J. Kraut, R. Hiesgen, A. Hinsch, D. Meissner and N. S. Sariciftci, *Adv. Funct. Mater.*, 2004, **14**, 1005.
53 X. Yang, J. Loos, S. C. Veenstra, W. J. H. Verhees, M. M. Wienk, J. M. Kroon, M. A. J. Michels and R. A. J. Janssen, *Nano Lett.*, 2005, **5**, 579.
54 M. Brinkmann and J. C. Wittmann, *Adv. Mater.*, 2006, **18**, 860.
55 G. Li, Y. Yao, H. Yang, V. Shrotriya, G. Yang and Y. Yang, *Adv. Funct. Mater.*, DOI: 10.1002/adfm.200600624.
56 H. Yang, T. J. Shin, L. Yang, K. Cho, C.Y. Ryu and Z. Bao, *Adv. Funct. Mater.*, 2005, **15**, 671.
57 J.-F. Chang, B. Sun, S. W. Brieby, M. M. Nielsen, T. I. Solling, M. Giles, I. McCulloch and H. Sirringhaus, *Chem. Mater.*, 2004, **16**, 4772.
58 J. Huang, G. Li and Y. Yang, *Appl. Phys. Lett.*, 2005, **87**, 112105.
59 V. Shrotriya, Y. Yao, G. Li and Y. Yang, *Appl. Phys. Lett.*, 2006, **89**, 063505.
60 V. D. Mihailetchi, H. Xie, B. de Boer, L. M. Popescu, J. C. Hummelen and P. W. M. Blom, *Appl. Phys. Lett.*, 2006, **89**, 012107.
61 V. D. Mihailetchi, H. Xie, B. de Boer, L. J. A. Koster and P. W. M. Blom, *Adv. Funct. Mater.*, 2006, **16**, 699.
62 V. D. Mihailetchi, L. J. A. Koster, P. W. M. Blom, C. Melzer, B. de Boer, J. K. J. van Duren and R. A. J. Janssen, *Adv. Funct. Mater.*, 2005, **15**, 795.
63 V. D. Mihailetchi, L. J. A. Koster, J. C. Hummelen and P. W. M. Blom, *Phys. Rev. Lett.*, 2004, **93**, 216601.
64 L. Onsager, *J. Chem. Phys.*, 1934, **2**, 599.
65 C. L. Braun, *J. Chem. Phys.*, 1984, **80**, 4157.
66 R. J. Kline, M. D. McGehee, E. N. Kdnikova, J. Liu and J. M. J. Frechet, *Adv. Mater.*, 2003, **15**, 1519.
67 A. Zen, J. Pflaum, S. Hirschmann, W. Zhang, F. Jaiser, U. Asawapirom, J. P. Rabe, U. Scherf and D. Neher, *Adv. Funct. Mater.*, 2004, **14**, 757.
68 D. Beljonne, J. Cornil, H. Sirringhaus, P. J. Brown, M. SHkunov, R. H. Friend and J. L. Bredas, *Adv. Funct. Mater.*, 2001, **11**, 229.
69 X. M. Jiang, R. Österbacka, O. Korovyanko, C. P. An, B. Horovitz, R. A. J. Janssen and Z. V. Vardeny, *Adv. Funct. Mater.*, 2002, **12**, 587.
70 P. Schilinsky, U. Asawapirom, U. Scherf, M. Biele and C. J. Brabec, *Chem. Mater.*, 2005, **17**, 2175.
71 C. Winder and N. S. Sariciftci, *J. Mater. Chem.*, 2004, **14**, 1077.
72 M. C. Scharber, D. Mühlbacher, M. Koppe, P. Denk, C. Waldauf, A. J. Heeger and C. J. Brabec, *Adv. Mater.*, 2006, **18**, 789.
73 L. J. Koster, V. D. Mihailetchi and P. W. M. Blom, *Appl. Phys. Lett.*, 2006, **88**, 093511.

74 J. Roncali, *Chem. Rev.*, 1997, **97**, 173.
75 (*a*) C. J. Brabec, C. Winder, N. S. Sariciftci, J. C. Hummelen, A. Dhanabalan, P. A. van Hal and R. A. J. Janssen, *Adv. Funct. Mater.*, 2002, **12**, 709; (*b*) F. Zhang, K. Jespersen, C. Bjorstrom, M. Svensson, M. R. Andersson, V. Sundstrom, K. Magnusson, E. Moons, A. Yartsev and O. Inganas, *Adv. Funct. Mater.*, 2006, **16**, 667; (*c*) D. Mühlbacher, M. Scharber, M. Morana, Z. Zhu, D. Waller, R. Gaudiana and C. Brabec, *Adv. Mater.*, 2006, **18**, 2884; (*d*) C. Shi, Y. Yao, Y. Yang and Q. Pei, *J. Am. Chem. Soc.*, 2006, **89**, 063505; (*e*) Y. Yao, C. Shi, G. Li, V. Shrotriya, Q. Pei and Y. Yang, *Appl. Phys. Lett.*, 2006, **89**, 153507.
76 (*a*) M. Hiramoto, M. Suezaki and M. Yokoyama, *Chem. Lett.*, 1990, **1990**, 327; (*b*) A. Yakimov and S. R. Forrest, *Appl. Phys. Lett.*, 2002, **80**, 1667.
77 J. Gilot, M. M. Wienk and R. A. Janssen, *Appl. Phys. Lett.*, 2007, **90**, 143512.
78 V. Shrotriya, E. H. Wu, G. Li, Y. Yao and Y. Yang, *Appl. Phys. Lett.*, 2006, **88**, 064104.
79 G. Li, C.-W. Chu, V. Shrotriya, J. Huang and Y. Yang, *Appl. Phys. Lett.*, 2006, **88**, 253503.
80 K. M. Coakley, Y. Liu, M. D. McGehee, K. L. Frindell and G. D. Stucky, *Adv. Funct. Mater.*, 2003, **13**, 301.





 